PHYSICAL REVIEW B VOLUME 26, NUMBER 6 15 SEPTEMBER 1982

Off-normal photoelectron diffraction study of the $c(2\times2)$ selenium overlayer on Ni(001)

D. H. Rosenblatt, S. D. Kevan,* J. G. Tobin, R. F. Davis,† M. G. Mason,‡ and D. A. Shirley
Materials and Molecular Research Division, Lawrence Berkeley Laboratory, University of California, Berkeley, California 94720 and Department of Chemistry, University of California, Berkeley, California 94720

J. C. Tang§ and S. Y. Tong
Department of Physics and Surface Studies Laboratory, University of Wisconsin—Milwaukee, Milwaukee, Wisconsin 53201

(Received 12 April 1982)

Off-normal energy-dependent photoelectron diffraction data are presented for the $c(2\times2)$ Se-Ni(001) system, and compared with calculations to confirm the accepted four-fold hollow-site geometry. The best agreement is found for a $d_\perp$ spacing of 1.55 Å, confirming earlier normal photoelectron diffraction and low-energy electron diffraction results. The size of the photoelectron diffraction modulations decreases with increasing polar angle of emission. An R-factor analysis indicates that the theory-to-experiment fit is very good, especially at smaller polar angles. Off-normal photoelectron diffraction is shown to be capable of distinguishing the correct site geometry for cases in which theoretical normal photoelectron diffraction curves for two geometries exhibit an "accidental coincidence" in peak positions.

I. INTRODUCTION

Photoelectron diffraction (PD) can be observed by measuring the angle-resolved photoemission intensity from a core level of an adsorbate atom or molecule bonded to a single-crystal metal surface. If the photon energy $h\nu$ is varied and the core-level photoelectrons are collected in the direction normal to the crystal face, diffraction of the photoelectrons can yield a strongly oscillatory dependence of the photoelectron intensity on kinetic energy. This specialized case of PD, termed normal photoelectron diffraction (NPD), has been used to determine the structures of overlayers adsorbed on metal surfaces.[1–6] The first experimental observation of NPD from a core level was made in 1978.[1] Dynamical scattering theory with calculated dipole matrix elements and phase shifts was used to analyze the data and illustrate their usefulness. This effect has now been observed in a large number of adsorbate-substrate systems and is found to be particularly suitable for accurate determination of the spacing between an adsorbate layer and the substrate ($d_\perp$). Structural information has been generally derived from a comparison of experimental and theoretical NPD curves,[1–7] although a more explicit method has been developed recently.[3,8] In this paper, we demonstrate for the first time that off-normal energy-dependent PD can also be used to derive accurate surface structures.

In an earlier paper,[4] we observed that the modulations in off-normal PD were not nearly as pronounced as those in NPD, making an accurate structural determination more difficult. In that work, off-normal data for the $c(2\times2)$ Se $3d$—Ni(001) system, taken at a coarse angular mesh, were presented. In this paper, we report off-normal PD curves of the same system, taken at intervals of 5° in polar angle, for two different azimuthal orientations. The finer angular mesh in the new data allows us to follow the evolution of the PD peaks with polar angle more carefully. More importantly, the experimental data have been fitted by multiple scattering theory, allowing an implicit structural determination of the adsorption site of the $c(2\times2)$ Se overlayer on Ni(001).

Section II contains experimental information. In Sec. III we briefly discuss the method and inputs of the multiple scattering calculations used to fit the experimental data. In Sec. IV we present and discuss the PD data. An R-factor analysis of the theory-to-experiment fit is presented in Sec. V, and conclusions from this work are given in Sec. VI.

II. EXPERIMENTAL

All the data reported here were obtained with an angle-resolved photoemission (ARP) spectrometer

described earlier.[9] The spectrometer has low-energy electron diffraction (LEED) and Auger-electron spectroscopy capabilities, as well as an adsorbate gas introduction system which allows for effusive beam dosing. The base pressure of the vacuum chamber was 2×10^{-10} Torr during all the measurements. The pressure rose to as high as 5×10^{-9} Torr during effusive beam dosing. The Ni(001) crystal was oriented to within 1° of the [001] direction. The crystal was cleaned by hot (1025 K) and room-temperature cycles of argon-ion sputtering followed by annealing to 875 K, resulting in a surface essentially free of impurities with a sharp (1×1) LEED pattern. The $c(2\times2)$ Se overlayer on Ni(001) was prepared by directing an effusive beam of H_2Se at the crystal, which was heated to 500 K. An exposure of 20—30 L was required to produce a sharp $c(2\times2)$ LEED pattern on Ni(001).

The experiments were performed on Beam Line I-1 at the Stanford Synchrotron Radiation Laboratory. Low-resolution ARP spectra were taken of the Se $3d$ level, which has a binding energy of 62 eV with respect to the vacuum level. Spectra were taken at intervals of 3 eV in photon energy. The angle-resolved relative intensity of this level was deduced by calculating the area of the core-level peaks (after background subtraction) and adjusting for photon flux and analyzer transmission. The kinetic energy range of the resulting PD curves was generally 40—200 eV. Experimental geometries are indicated in the figures.

III. THEORY

The multiple scattering theory used to calculate the photoemission intensity versus energy (IE) curves was described earlier.[7,10] The $3d$ initial-state wave function of Se was obtained from a self-consistent $X\alpha$ scattered-wave calculation of a Ni_5Se cluster. Dipole transition matrix elements were calculated at each photon energy. The final state was calculated at each kinetic energy by a Green's-function method corresponding to the $c(2\times2)$ Se-Ni(001) slab geometry. All multiple scattering of the photoelectron was included until numerical convergence was reached.

Inputs to the multiple scattering method include: (1) substrate (nickel) phase shifts obtained from the self-consistent band-structure potential of Wakoh,[11] and (2) Se phase shifts obtained from the same $X\alpha$ scattered-wave calculation that generated the Se $3d$ wave function. The imaginary part of the optical potential (in eV) for the final state was taken to be

$$V_I=3.8\left[\frac{E+V_0}{90+V_0}\right]^{1/3},$$

where E is the energy in eV above the vacuum. The inner potential used was $V_0=13.2$ eV. Earlier, we had used $V_0=11.2$ eV for Se on Ni(001),[12] but the R-factor analysis described in Sec. V gave a slightly better value for $V_0=13.2$ eV. For example, the normalized R factor at the optimal structure (see Sec. V) is 0.789 for $V_0=11.2$ eV and 0.760 for $V_0=13.2$ eV, indicating a 4% improvement. Although the 2-eV shift slightly improved the R factor, the same $d_\perp$ spacing was chosen by either $V_0=11.2$ or 13.2 eV.

The Se $3d$ level was placed at 62 eV below vacuum. Calculations of the IE curves were made for the same energy range as the data, i.e., 40—200 eV. The Se atom was placed at the fourfold hollow site at Se-Ni perpendicular spacings ($d_\perp$) of 1.45, 1.55, 1.65, and 1.75 Å. Earlier analyses have convincingly shown that the adsorption site is the fourfold hollow.[2,4,12–14] In this study, we did not place the Se at other binding registries, except for $d_\perp=2.34$ Å in the top site (see Sec. IV and Fig. 4).

IV. RESULTS AND DISCUSSION

In an earlier paper,[4] we presented limited off-normal photoelectron diffraction data on $c(2\times2)$ Se-Ni(001). In that work, data were taken for emission into the [100] azimuth at polar angles of 15°, 30°, and 45°, and into the [110] azimuth at polar angles 18°, 36°, and 54°. The curves were rich in structure, but the intensity modulations were much smaller than those at normal emission. When the photoemission is normal, waves scattered to the detector by atoms arranged symmetrically around the emitting atom interfere constructively with each other at the detector. Therefore, the conditions of constructive interference between the direct wave and the wave scattered by each of these symmetrically arranged neighbors are the same, leading to a series of large, well-separated peaks in the NPD curve. However, at off-normal angles of emission, the conditions of constructive interference between direct and scattered waves are different for each of these neighbor atoms, leading to a collection of overlapping peaks. Consequently, as the detector is rotated off normal, new peaks are seen, and the overall peak-to-valley ratio decreases. The latter can be seen in Fig. 1, where PD curves are shown for emission in the [100] azimuth

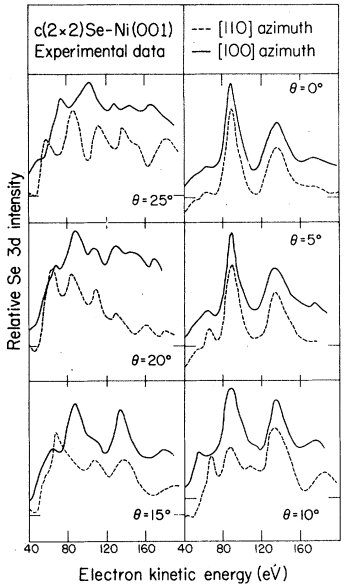

FIG. 1. Experimental PD data for $c(2\times2)$ Se $3d$ — Ni(001) for emission in the [100] azimuth (solid curves) and the [110] azimuth (dashed curves) as a function of polar angle θ. The experimental geometries for the [100] and [110] azimuths are shown in Figs. 2 and 3, respectively.

with polar angles $\theta=0°$, 5°, 10°, 15°, 20°, and 25°. The experimental geometry for this data set is shown in Fig. 2. The NPD curve ($\theta=0°$) exhibits the greatest peak-to-valley ratio. As the detector is rotated off-normal, the modulations get smaller.

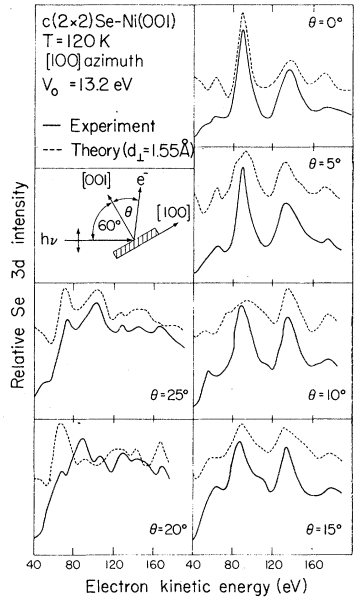

FIG. 2. Experimental PD data for the [100] azimuth (solid curves) compared with theoretical calculations for the hollow site with $d_\perp=1.55$ Å (dashed curves).

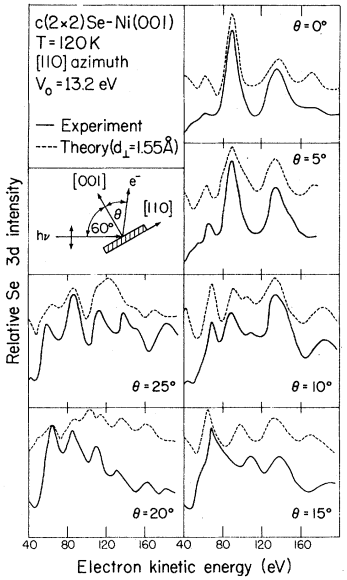

FIG. 3. Experimental PD data for the [110] azimuth (solid curves) compared with theoretical calculations for the hollow site with $d_\perp=1.55$ Å (dashed curves).

At $\theta=25°$, the modulations are small enough that the underlying atomic cross section is becoming apparent. An example of a new peak which emerges at off-normal emission is seen in Fig. 1. This peak is first seen at $\theta=10°$ in the [100] azimuth at 111-eV kinetic energy, and becomes the most prominent feature in the NPD curve by $\theta=25°$. The peak disperses from 111 eV at $\theta=10°$ to 103 eV at $\theta=25°$. The main peaks present in the PD curve at normal emission (kinetic energy 89 and 138 eV) decrease in intensity while dispersing slightly in energy with polar angle.

Similar effects are seen if the crystal is rotated azimuthally about the sample normal by 45°, so that the photon beam and emission direction are both located in the [110] azimuth. This experimental geometry is shown in Fig. 3. These experimental PD curves are also shown in Fig. 1. Again, the peak-to-valley contrast is greatest at normal emission. The two main peaks in the normal emission curve are at kinetic energy 89 and 137 eV. A new peak at 110 eV appears at $\theta=10°$ and grows in intensity through $\theta=25°$.

A comparison between the PD curves for the two azimuths studied is of interest at this point. For core-level emission from an adsorbate in a fourfold hollow site (C_{4v} symmetry), the PD intensity at normal emission is independent of the azimuthal angle ϕ of the incident photon beam. Thus, the two curves at $\theta=0°$ of Fig. 1 indicate the high degree of reproducibility of the data at

equivalent but nonidentical conditions. As the detector is moved off normal, we are comparing two sample geometries which differ by 45° not only in the azimuthal orientation of the photon polarization vector, but also in the azimuthal orientation of photoelectron emission. The second effect induces significant differences between pairs of curves with the same polar angle, especially for $\theta \geq 15°$. At $\theta = 5°$ the differences are minor, and at $\theta = 10°$ the major difference is in the position of the first PD peak. At $\theta = 15°$ and 20°, the curves are still similar above 90-eV kinetic energy. Only at $\theta = 25°$ do PD curves for the two azimuths look substantially different at all energies.

We now turn to the theoretical analysis of the data in Fig. 1. The data for the [100] azimuth are reproduced in Fig. 2 and compared with PD calculations for Se in the fourfold hollow site at $d_\perp = 1.55$ Å, where $d_\perp$ is the perpendicular distance between the $c(2\times2)$ Se overlayer plane and the nickel surface. The agreement is quite good for all angles sampled. Visual inspection indicates that the quality of the fit is extremely good at small polar angles ($\theta \leq 15°$) but worsens somewhat at the larger polar angles sampled. Theoretical calculations for emission into the [110] azimuth are shown in Fig. 3 along with the experimental curves, which are reproduced from Fig. 1. Calculated PD curves for Se in the fourfold hollow site with $d_\perp = 1.55$ Å are presented. The fit with the experimental data is again quite good. Just as for the [100] azimuth, the fit is excellent for smaller polar angles and deteriorates as θ gets large. An *R*-factor analysis was carried out for the $d_\perp$ values of 1.45, 1.55, 1.65, and 1.75 Å using all data from both azimuths studied. The $d_\perp = 1.55$ Å spacing was found to give the optimum (lowest) *R* factor. Details of the *R*-factor analysis are given in the next section. The determination of $d_\perp = 1.55$ Å is in excellent agreement with our previous NPD study on this system[4] and with LEED intensity analyses in the literature.[13,14]

A major benefit of studying off-normal photoelectron diffraction is that a comparison of many experimental curves to theory provides a self-consistency check of the NPD results, in the same manner that LEED intensity analysis at off-normal incidences can be used to confirm results obtained by studying the LEED beams at normal incidence. At the same time, caution should be taken in examining the PD fits at large polar angles, as both experimental and calculated curves exhibit smaller oscillations and it is more difficult to establish whether a good fit exists. The peak positions and intensities change more rapidly with angle at large polar angles because there are more inequivalent atoms around the emitting site. Consequently, small errors in the measurement of the polar angle will cause shifts in the NPD peaks which reduce the quality of the theory-to-experiment fit at large polar angles.

The close similarity between all six experimental PD curves with $\theta \leq 10°$ ($\theta = 0°$, 5°, and 10° in both azimuths) presents the possibility that NPD data could be taken into a much larger solid angle of emission (resulting in a dramatic reduction of data collection time) without significantly degrading the structural accuracy of NPD. In a previous paper,[4] we used NPD to determine that selenium is situated above the hollow sites on Ni(001) with $d_\perp = 1.55 \pm 0.04$ Å. In that study (as well as this work), the angular acceptance of our electron-energy analyzer was a half angle of 3°. If the angular acceptance is increased to 10° half angle, the number of photoelectrons collected will increase by more than 10 times if one assumes an isotropic angular distribution of photoelectrons over the range $0° \leq \theta \leq 10°$. We estimate that the corresponding decrease in structural accuracy will be considerably less than the current experimental error; i.e., the increased angular acceptance should introduce an additional error of about ± 0.02 Å to the $d_\perp$ determination for Se on Ni(001). We conclude that future NPD experiments could benefit from the use of a larger angular acceptance of photoelectrons.

Occasionally, the theoretical NPD curves for two different sites exhibit an "accidental coincidence" in peak positions which makes it more difficult to distinguish the correct site geometry. In these cases, most or all of the peaks in one curve have energy positions which differ by 5 eV or less from the energies of peaks in the second curve. For example, in an earlier paper, Li and Tong[15] noted that for normal emission from the $c(2\times2)$ Se-Ni(001) system, there is an accidental coincidence of diffraction peaks between $d_\perp = 1.55$ Å (hollow site) and $d_\perp = 2.34$ Å (top site). These authors expected that this accidental coincidence would be lifted when off-normal emission data became available. This is indeed the case, and we show in Fig. 4 the comparison at $\theta = 15°$ of experimental data with calculated PD curves for $d_\perp = 1.55$ Å (hollow site) and $d_\perp = 2.34$ Å (top site). The emission direction is along the [100] azimuth. The peak at 88 eV of the hollow site curve is split into two peaks (80 and 100 eV) in the top site curve. Near 88 eV, there is a valley for the top site. This comparison definitely rules out the top

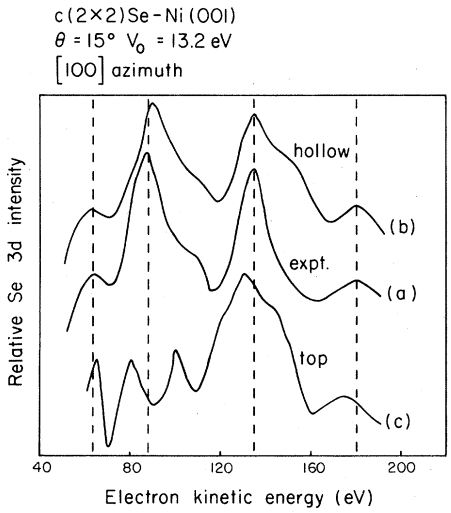

FIG. 4. Comparison of (a) experimental PD data for $c(2\times2)$ Se $3d-$Ni(001) with calculated curves for (b) Se in the hollow site, $d_\perp=1.55$ Å and (c) Se in the top site, $d_\perp=2.34$ Å. The polar angle of emission is $\theta=15°$ in the [100] azimuth.

site as the binding location of $c(2\times2)$ Se on Ni(001).

V. *R*-FACTOR ANALYSIS

To facilitate comparison between theory and experiment, and to compare the "fit" obtained here with other structural analyses, we performed an *R*-factor analysis on this system. We used a normalized *R* factor,[16] described earlier, which was based on individual *R* factors defined by Van Hove *et al.*,[17] Zanazzi and Jona,[18] and Pendry.[19] The normalized *R* factor is defined by

$$R_N=\tfrac{1}{6}(R_1+R_2+R_3+R_4+R_5+R_6)\ , \tag{1}$$

where

$$R_1=A_1\frac{\Delta E_s}{\Delta E_{\rm tot}}\ , \tag{2}$$

where ΔE_s is the energy range with slopes of opposite signs and $\Delta E_{\rm tot}$ is the total energy range,

$$R_2=A_2\int(I_e-cI_t)^2dE\ , \tag{3}$$

$$R_3=A_3\int(I_e'-cI_t')^2dE\ , \tag{4}$$

$$R_4=A_4\int(I_e''-cI_t'')^2dE\ , \tag{5}$$

$$R_5=A_5\int\frac{|I_e'-cI_t'|\,|I_e''-cI_t''|}{|I_e'|+\max|I_e'|}dE\ , \tag{6}$$

$$R_6=A_6\frac{\int(Y_e-Y_t)^2dE}{\int(Y_e^2+Y_t^2)dE}\ . \tag{7}$$

Here, I_e are the experimental intensity data, I_e' and I_e'' refer to the first and second derivatives of I_e with respect to energy. I_t, I_t', and I_t'' are the corresponding quantities for the calculated intensities. Also,

$$c=\frac{\int I_e dE}{\int I_t dE}\ , \tag{8}$$

$$Y_{e,t}=\frac{I_{e,t}'/I_{e,t}}{1+V_I^2(I_{e,t}'/I_{e,t})^2}\ . \tag{9}$$

where V_I is defined in Sec. III.

The weights $A_1,\ldots,A_6$ are chosen such that the average value of each *R* factor over the geometries considered in this work is 1.0. This ensures that the influence of each *R* factor is roughly the same, so that in R_N, no one *R* factor dominates the others.

The value of R_N, evaluated over the 11 PD curves shown in Figs. 2 and 3 (the two $\theta=0°$ curves are degenerate, so we took only the one in Fig. 2), is plotted as a function of $d_\perp$ in Fig. 5. A well-defined minimum is seen at $d_\perp=1.55$ Å. This result agrees with the determination by visual judgment, and it also agrees with earlier PD analysis at normal emission and with LEED.[13,14]

To compare the degree of fit with other structural analyses, the value of the Zanazzi-Jona *R* factor[20] ($R_{\rm ZJ}$) for $d_\perp=1.55$ Å is 0.05. From previous experience, a structural analysis is acceptable if $R_{\rm ZJ}<0.2$. With this criterion, the overall fit here is substantially above average.

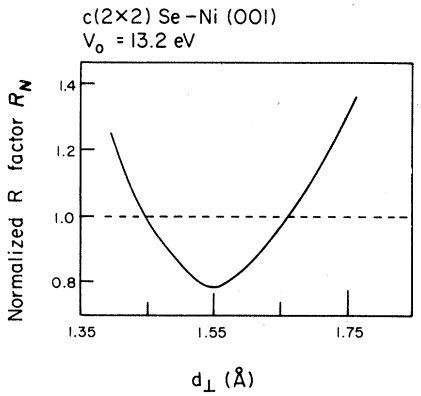

FIG. 5. Plot of the normalized *R* factor vs $d_\perp$ spacing.

VI. CONCLUSIONS

In this paper, we have demonstrated, for the first time, the use of off-normal energy-dependent photoelectron diffraction curves to determine surface structure. Off-normal PD curves show smaller oscillation amplitudes than NPD curves, but these curves can nevertheless be used to accurately determine the structural parameter $d_\perp$. In the event of an accidental coincidence at normal emission, we have demonstrated that off-normal PD curves can be used to resolve the coincidence. Owing to the rapid decrease of the amplitude of the oscillations at larger θ, the most useful range seems to be between $\theta=0°$ and 15°.

ACKNOWLEDGMENTS

We wish to thank Mrs. Winifred Heppler for the preparation of the nickel crystal. The work of one of us (J.G.T.) was supported by an NSF Fellowship. This work was supported by the Director, Office of Energy Research, Office of Basic Energy Sciences, Chemical Sciences Division of the U.S. Department of Energy under Contract No. DE-AC03-76SF00098. It was performed at the Stanford Synchrotron Radiation Laboratory, which is supported by the NSF through the Division of Materials Research. Work at the University of Wisconsin—Milwaukee was supported by NSF Grant No. DMR 8101203 and Petroleum Research Fund Grant No. 11584-AC 5,6.

---

*Permanent address: Bell Laboratories, Murray Hill, NJ 07974.

†Permanent address: Research Laboratories, Polaroid Corporation, Waltham, MA 02154.

‡Permanent address: Research Laboratories, Eastman Kodak Company, Rochester, NY 14650.

§Permanent address: Department of Physics, University of Zheijiang, Hangzhou, People's Republic of China.

[1]S. D. Kevan, D. H. Rosenblatt, D. Denley, B.-C. Lu, and D. A. Shirley, Phys. Rev. Lett. 41, 1565 (1978).

[2]C. H. Li and S. Y. Tong, Phys. Rev. Lett. 42, 901 (1979).

[3]D. H. Rosenblatt, J. G. Tobin, M. G. Mason, R. F. Davis, S. D. Kevan, D. A. Shirley, C. H. Li, and S. Y. Tong, Phys. Rev. B 23, 3828 (1981).

[4]S. D. Kevan, D. H. Rosenblatt, D. R. Denley, B.-C. Lu, and D. A. Shirley, Phys. Rev. B 20, 4133 (1979).

[5]S. D. Kevan, R. F. Davis, D. H. Rosenblatt, J. G. Tobin, M. G. Mason, D. A. Shirley, C. H. Li, and S. Y. Tong, Phys. Rev. Lett. 46, 1629 (1981).

[6]S. Y. Tong and C. H. Li, Crit. Rev. Solid State Sci. 10, 209 (1981).

[7]C. H. Li, A. R. Lubinsky, and S. Y. Tong, Phys. Rev. B 17, 3128 (1978).

[8]Z. Hussain, D. A. Shirley, S. Y. Tong, and C. H. Li, Proc. Natl. Acad. Sci. USA 78, 5293 (1981).

[9]S. D. Kevan and D. A. Shirley, Phys. Rev. B 22, 542 (1980).

[10]S. Y. Tong, C. H. Li, and A. R. Lubinsky, Phys. Rev. Lett. 39, 498 (1977).

[11]S. Wakoh, J. Phys. Soc. Jpn. 20, 1894 (1965).

[12]C. H. Li and S. Y. Tong, Phys. Rev. Lett. 43, 526 (1979).

[13]M. Van Hove and S. Y. Tong, J. Vac. Sci. Technol. 12, 230 (1975); S. Andersson, J. B. Pendry, B. Kasemo, and M. Van Hove, Phys. Rev. Lett. 31, 595 (1973).

[14]J. E. Demuth, D. W. Jepsen, and P. M. Marcus, Phys. Rev. Lett. 31, 540 (1973).

[15]C. H. Li and S. Y. Tong, Phys. Rev. B 19, 1769 (1979).

[16]S. Y. Tong and K. H. Lau, Phys. Rev. B 25, 7382 (1982).

[17]M. A. Van Hove, S. Y. Tong, and M. H. Elconin, Surf. Sci. 64, 85 (1977).

[18]E. Zanazzi and F. Jona, Surf. Sci. 62, 61 (1977).

[19]J. B. Pendry, J. Phys. C 13, 937 (1980).

[20]Our R_5 is derived from the Zanazzi-Jona R factor (Ref. 18), except for a different coefficient A_5.